Investigations of the impact of heating schemes and poloidal asymmetries on the heavy impurity transport in AUG and TCV

A. Jardin[1], D. Mazon[2], F. Jaulmes[3], R. Bilato[4], C. Angioni[4], K. Król[1], D. Colette[2], G. Vogel[4], ASDEX Upgrade Team[5], TCV Team[6], and EUROfusion MST1 Team[7]

[1]Institute of Nuclear Physics Polish Academy of Sciences (IFJ PAN), PL-31-342, Krakow, Poland

[2]CEA, IRFM, F-13108 Saint-Paul-lez-Durance, France

[3]Institute of Plasma Physics of the CAS, Prague, Czech Republic

[4]Max-Planck-Institut fuer Plasmaphysik, Boltzmannstrasse 2, 85748 Garching, Germany

[5]See the author list of H. Meyer et al, Nucl. Fusion 59 (2019) 112014

[6]See the author list of S. Coda et al, Nucl. Fusion 59 (2019) 112023

[7]See the author list of B. Labit et al, Nucl. Fusion 59 (2019) 086020

1. Introduction

Modern tokamaks move from carbon to tungsten (W) as plasma-facing material due to the tritium retention issue in ITER. However, W impurities are a major source of concern due to radiation losses in the plasma core and W concentration must be kept at acceptable levels, typically $c_W \lesssim 10^{-4}$ [1]. Besides, impurity poloidal asymmetries, induced *e.g.* by ICRH or NBI, can significantly affect the radial impurity transport [2], indicating that efficient W mitigation strategies should include the effect of these asymmetries. We report here recent experiments and analysis performed under the MST1 Topic 10 to address these issues [3]. A series of AUG H-mode discharges were performed to study W transport in helium (He) and deuterium (D) plasmas, including the impact of different ICRH and NBI waveforms on the induced soft X-ray (SXR) asymmetries, with the help of W controlled injection by laser blow-off (LBO). Besides, a transient up-down SXR asymmetry has been observed in TCV plasmas with ECRH, following controlled gas injections with the disruption mitigation valve (DMV).

2. AUG analysis

Two successful plasmas discharges #37615, #37640 were performed on AUG in D in 2020, with W LBO injections. We focus here on the shot #37640, which allows a direct comparison with AUG #36713 in He, with a plasma current $I_p = 0.6$ MA and toroidal magnetic field $B_t = 2.64$ T, corresponding to a low-field side (LFS) deposition of ICRH at 36.5 MHz (r/a ~ 0.3). The time traces of heating and radiated power are displayed in Fig. 1 (left), with the W LBOs clearly visible in the radiated power. The radiated power is significantly higher in #36713 (He) than in #37640 (D) due to higher W content in the He plasma.
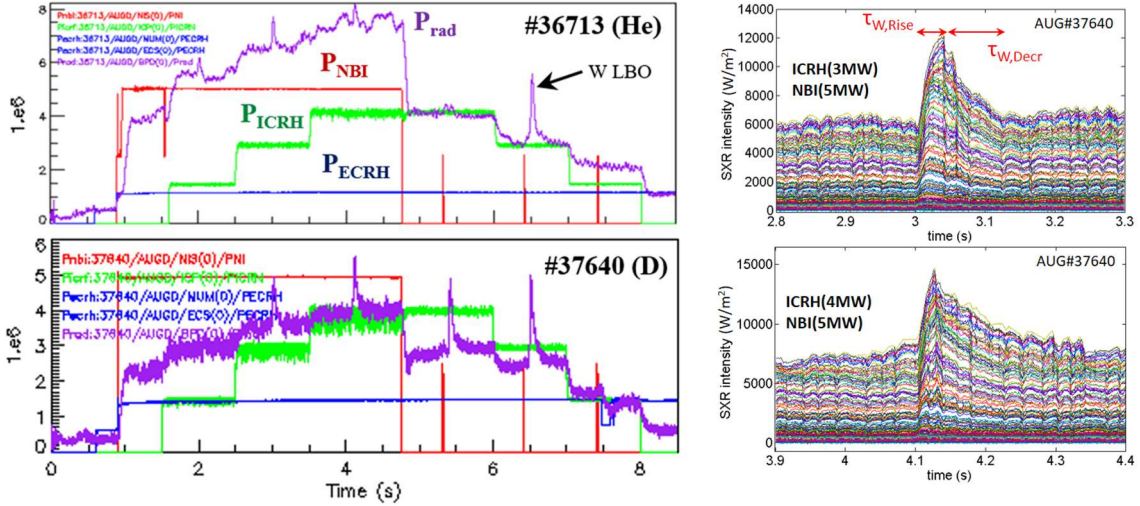
Figure 1. Left: Time traces of radiated power, ECRH, ICRH and NBI powers for AUG #36713 and #37640.
Right: SXR time traces of two W LBOs performed in AUG #37640.

The W LBO phases are examined with the SXR diagnostic, as depicted in Fig. 1 (right). In the considered experiments, the rising time of W signal after LBO was stable with $\tau_{W,Rise} \sim 20 - 30\ ms$, while the decrease time $\tau_{W,Decr} \sim 50 - 200\ ms$ depending on plasma conditions. Notably, $\tau_{W,Decr}$ increased with P$_{ICRH}$ but the impact of NBI was not clear. These observations were confirmed by the SPRED (W^{44+}, 13.3 nm) diagnostic. In the presence of ICRH and NBI, the poloidal distribution of impurities $\tilde{n}_Z$ is governed by [4]:

$$\frac{\tilde{n}_Z}{\langle n_Z \rangle} = 2\frac{r}{R_0}\cos(\theta)\left[\frac{m_Z \Omega^2 R_0}{2T_i}\left(1 - \frac{Zm_i}{m_Z}\frac{Z_{eff}T_e}{Z_{eff}T_e + T_i}\right) - \frac{Zf_m}{2}\frac{T_e}{Z_{eff}T_e + T_i}\left(\frac{T_\perp}{T_\parallel} - 1\right)\right] \tag{1}$$

where in particular Ω denotes the toroidal rotation and $T_\perp/T_\parallel$ is the anisotropy temperature ratio of the minority species. The estimation of $T_\perp/T_\parallel$ could be performed using the TORIC-SSFPQL code, as presented in Fig. 2.
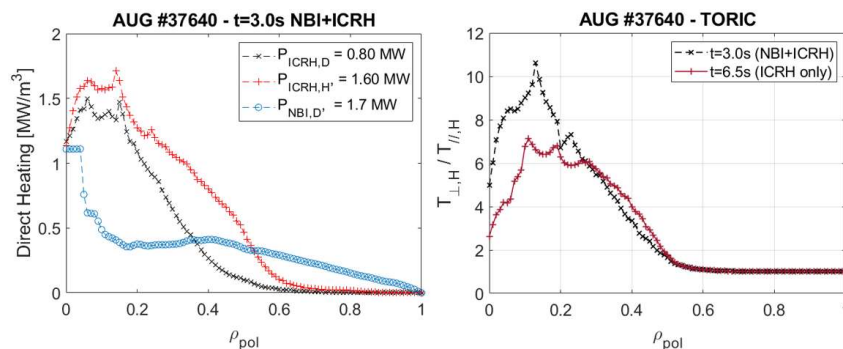

Figure 2. Left: TORIC simulation of power deposition profiles for AUG #37640 @3.0s.
Right: estimated anisotropy temperature ratios for AUG #37640 @3.0s and @6.5s.

Using the plasma temperature and rotation profiles obtained from CXRS and IDA/IDI analysis, Eq. (1) allowed to estimate the expected level of W in-out asymmetry and compare with experimental SXR tomographic inversions, as shown in Fig. 3. A clear HFS SXR

asymmetry is visible @6.5s at r/a ~ 0.1 – 0.4 with ICRH only, while @3.0s with NBI/ICRH competition, no significant in-out asymmetry is observed.
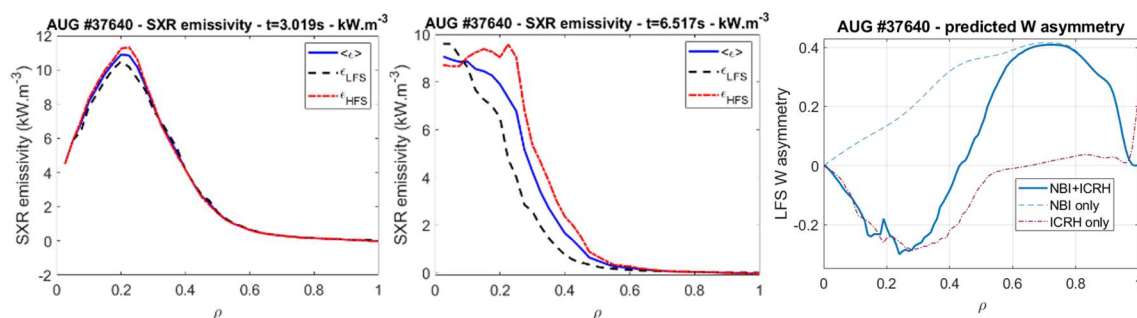

Figure 3. Left and Middle: flux-surface averaged SXR emissivity profiles for AUG #37640 @3.0s and @6.5s, just after W LBO. Right: predicted W LFS asymmetry from Eq. (1).

A comparison between #37640 in D and #36713 in He is presented in Fig. 4. As shown by TORIC, the $T_\perp/T_{//}$ is predicted to be higher in He, resulting in a larger HFS W asymmetry. This difference in confirmed by the SXR tomographic inversions, as displayed in Fig 4 (right). As a perspective, the analysis could now be focused on the determination of experimental W transport coefficients [5] and comparison with models such as NEO.
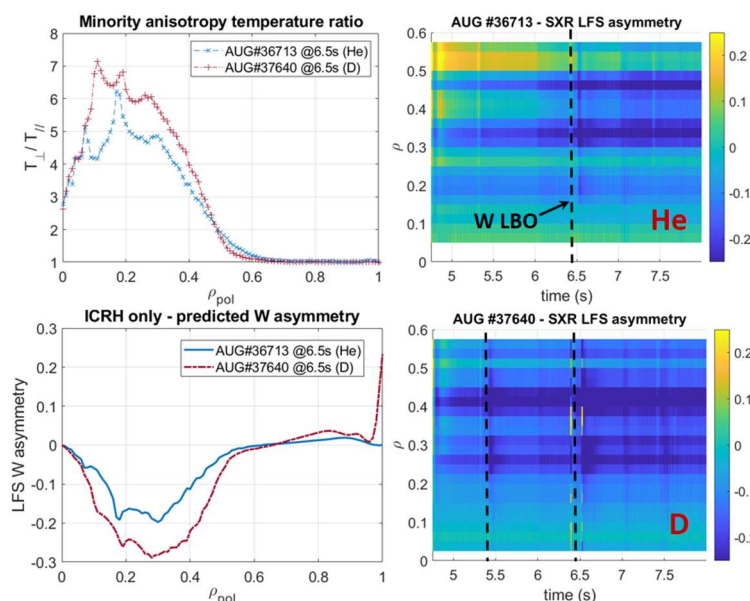

Figure 4. Left: predicted minority anisotropy temperature ratio and W in-out asymmetry for AUG #37640 and #36713 @6.5s. Right: Experimental SXR LFS asymmetry by 2D tomography.

3. Observations on TCV

A series of L-mode D plasma were performed with I_p = 100 kA, B_t = 1.3 T and pure ECRH heating with two phases: P_{ECRH} = 0.8 – 1.6 MW (0.3 – 1.3 s) and on-axis or off-axis (r/a ~ 0.4) deposition. Fast Neon and Krypton injections were performed with the DMV system to study impurity transport and asymmetries, in the absence of rotation and temperature anisotropy (from NBI and ICRH), as monitored by the SXR diagnostic, see Fig. 5. Using

SXR background subtraction, transient up-down asymmetries were observed in the 5 – 20 ms following the DMV opening, as presented in Fig. 6. It was observed that the location of the asymmetry could vary depending on the conditions of the injection, especially neon or krypton. Further studies with the code developed in [6] are foreseen to investigate the origin of these transient asymmetries.
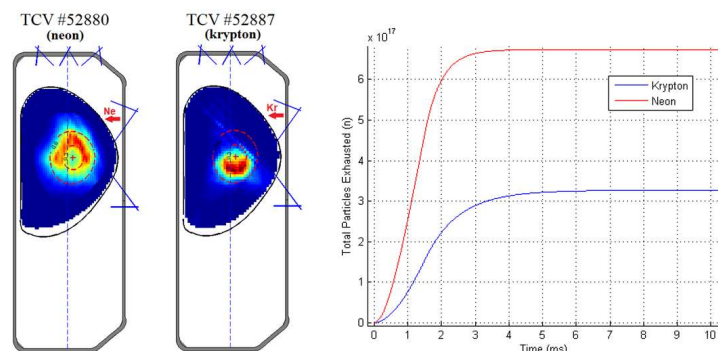

Figure 5. Left: Observed up-down SXR asymmetry after background subtraction on TCV, following gas injections with the DMV. Right: prediction of the time evolution of particle exhaust from the DMV.
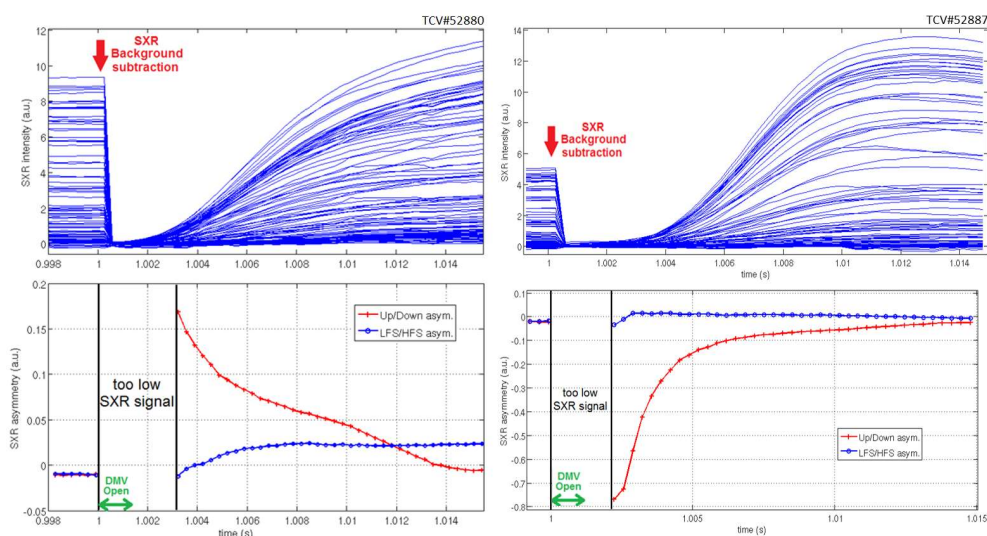

Figure 6. Time traces of SXR channels brightness (top), up/down and LFS/HFS SXR asymmetry by tomography (bottom) for TCV #52880 with Neon injection (left) and #52887 with Krypton injection (right).

[1] T. Puetterich et al., Nucl. Fusion 50 (2010) 025012.
[2] C. Angioni et al, Nuclear Fusion 54 (2014) 083028.
[3] D. Mazon et al, MST1-T10 AUG & TCV experiments report, 2019-2020.
[4] M. L. Reinke et al, Plasma Phys. Control. Fusion 54 (2012) 045004.
[5] M. Sertoli et al, Physics of Plasmas 24 (2017) 112503.
[6] P. Maget et al., Plasma Phys. Control. Fusion 62 (2019) 025001.